

The intelligent Photomultiplier Tubes for OSIRIS

Feng Gao,^{a,1} Tim Kuhlbusch,^a Achim Stahl,^a Jochen Steinmann,^{a,2} Cornelius Vollbrecht^{a,b} and Christian Wysotzki^a

^a*Physics Institute 3B, RWTH Aachen University, Aachen, Germany*

^b*Nuclear Physics Institute IKP-2, Forschungszentrum Jülich GmbH, Jülich, Germany*

E-mail: jochen.steinmann@physik.rwth-aachen.de

ABSTRACT: The dimensions of liquid scintillator neutrino detectors have grown over the years. Thus, the analog cable length required for the readout increases. In consequence, the signal loss increases as well. With the intelligent Photomultiplier Tube this problem can be solved. The digitiser is moved as close as possible to the Photomultiplier Tube. This concept allows nearly lossless digitisation of the analog signal. Furthermore, a computing unit next to the analog-to-digital converter enables implementation of on-the-fly data processing and control algorithms. This paper presents the detailed concept and the performance of the intelligent Photomultiplier Tube.

KEYWORDS: Photon detectors for UV, visible and IR photons (vacuum), Data acquisition concepts, Large detector systems for particle and astroparticle physics, Performance of High Energy Physics Detectors

¹Now at Université libre de Bruxelles, Brussels, Belgium.

²Corresponding author.

Contents

1	Introduction	1
2	OSIRIS	2
3	Concept of the intelligent PMT	2
4	Implementation of the intelligent PMT	3
4.1	Photomultiplier Tubes	3
4.2	Voltage Divider (Base)	3
4.3	High Voltage Board	4
4.4	Readout Board	5
4.5	Slow Control and Configuration Unit	6
4.6	Power Over Ethernet	6
4.7	Cable	6
4.8	Potting & Holder	7
5	Surface Board	7
5.1	LED & Laser Trigger	8
5.2	Synchronisation	9
6	Slowcontrol of the iPMT system	9
7	Performance of a single iPMT	10
7.1	Charge characteristics	10
7.2	Characteristics of the waveform maximum	12
7.3	Self triggered charge spectrum	13
8	Summary / Conclusions	15

1 Introduction

The **Jiangmen Underground Neutrino Observatory (JUNO)** experiment is a dedicated neutrino detector currently under construction in southern China [1]. The detection mechanism is based on neutrino interactions with liquid scintillator (LS). A highly radiopure LS is of foremost importance for the success of JUNO [2]. Therefore, the dedicated **Online Scintillator Intrinsic Radioactivity Investigation System (OSIRIS)** experiment monitors the radiopurity of the scintillator during filling of JUNO.

OSIRIS uses a novel Photomultiplier Tube (PMT) integration scheme – called intelligent PMT (iPMT) – to detect light from radioactive decays. The concept, realisation and performance of the iPMT system is presented in this paper.

Due to unforeseen problems and the necessary repairs of the iPMTs, they are not installed in the first phase of OSIRIS. They will be used in the future upgrade of OSIRIS focusing on the search for solar pp neutrinos [3].

2 OSIRIS

The OSIRIS experiment is a facility to monitor the internal radiopurity of the scintillator used in the JUNO experiment during filling. For this purpose, a fraction of the LS is fed continuously into OSIRIS [4]. The commissioning of the LS purification systems of JUNO is also monitored by OSIRIS.

The detector is separated into the inner detector, which consists of the LS contained in the acrylic vessel and the outer detector, that uses the shielding water as a Cherenkov muon veto. The light produced in both detector parts is detected by PMTs. The outer detector is instrumented by 12 PMTs. Further 64 PMTs are pointing towards the center of the acrylic vessel (cf. Figure 1).

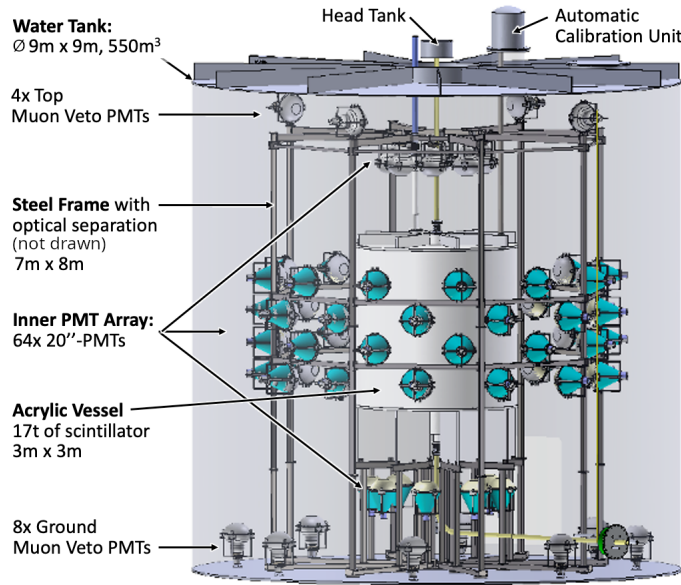


Figure 1: Layout of the OSIRIS detector [4].

3 Concept of the intelligent PMT

For the readout of large liquid scintillator detectors, long analog cables have been used in the past. For example, Borexino uses a cable length of 57 m for all PMTs [5, p. 12]. A comparable cable length is used in the SuperKamiokande detector [6]. If the size of the detector gets larger, the length of those cables increases. Thus, the attenuation along these cables increases as well.

Assuming an RG58 cable with typical attenuation at 100 MHz of 12 dB/100 m. At a length of 60 m the output voltage is reduced to 43.6% at 100 MHz. The attenuation depends on the frequency. Typically, the high frequencies are attenuated more, resulting in a shaping of the signal. Recovery of the original signal is only possible with enormous effort. The attenuated frequencies have to be amplified to compensate the attenuation. In case the amplification and the attenuation do not match, the original signal is not recovered.

The idea behind the concept of the iPMTs is to move digitiser and readout as close as possible to the PMT. By this, the analog signal path can be reduced to a few centimeters. With the digital output, the cable length no longer has an impact on the quality of the data. The length of the digital cable is limited as well, but the digital signals can be refreshed without loss of information.

In order to handle the digitised data, a signal processing unit is inserted at the back of each single PMT as illustrated in Figure 2. The processing unit packs the digitised data into waveforms, which are transmitted digitally via Ethernet. In addition, this unit provides resources for data reduction or reconstruction. Also high level algorithms, e.g. a stabilisation of the gain of the PMT, can be implemented on the processing unit.

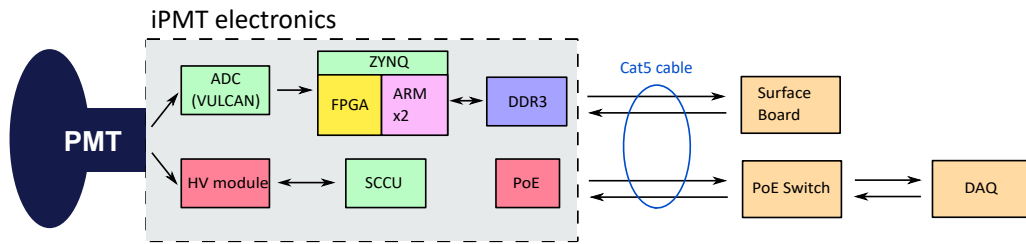


Figure 2: Overview of iPMT electronics.

The waveforms are transmitted on a self-triggered basis. If the processing unit detects a pulse in the waveform by e.g. a simple threshold discriminator or more advanced pulse detection techniques, this waveform packet is sent to the data acquisition (DAQ). Inside the DAQ software, a global trigger and event building is implemented and noise hits are discarded.

The whole readout concept was initially developed for usage in the JUNO central detector [7]. After it became clear that the concept is not going to be used for this detector, the whole concept was iterated again. This second iteration is presented in this paper.

4 Implementation of the intelligent PMT

In the following sections, each component of the iPMT – from the PMT to the DAQ – is described in more details. A complete assembly of an iPMT electronics stack is depicted in Figure 3.

4.1 Photomultiplier Tubes

For OSIRIS, 76 dynode photomultipliers of the type R15343 from Hamamatsu Photonics were prepared.

The PMTs are comparable to the Hamamatsu R12860HQ regarding the dimensions and performance. OSIRIS's PMTs can be separated into two groups, the PMTs looking inwards towards the acrylic vessel, and those, which monitor the water pool and serve as a muon veto. 12 PMTs are selected for the muon veto. The selection is based on the data given by Hamamatsu (cf. Figure 4). There are eight PMTs with transition time spread (TTS) of 2.8 ns or more. These PMTs are selected for the veto. The remaining four PMTs are the ones, which have the highest dark count rate.

4.2 Voltage Divider (Base)

The voltage divider follows the reference design by Hamamatsu with a few modifications. For a safe operation, the clearance between the high voltage (HV) and the ground traces is adapted according

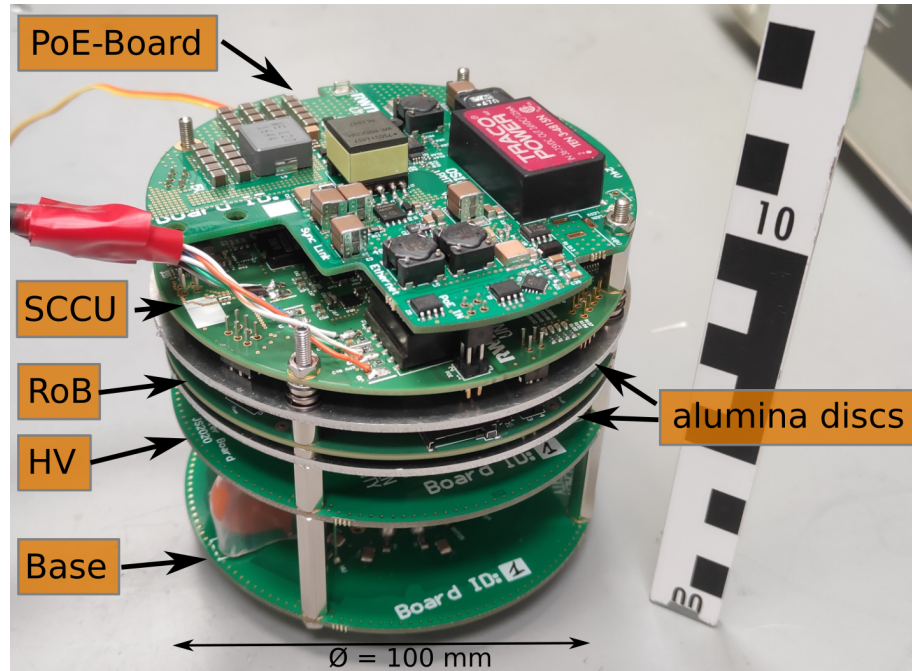


Figure 3: Image of an iPMT electronics stack. Alumina discs are placed above and below the Readout Board (ROB) for a better heat transfer.

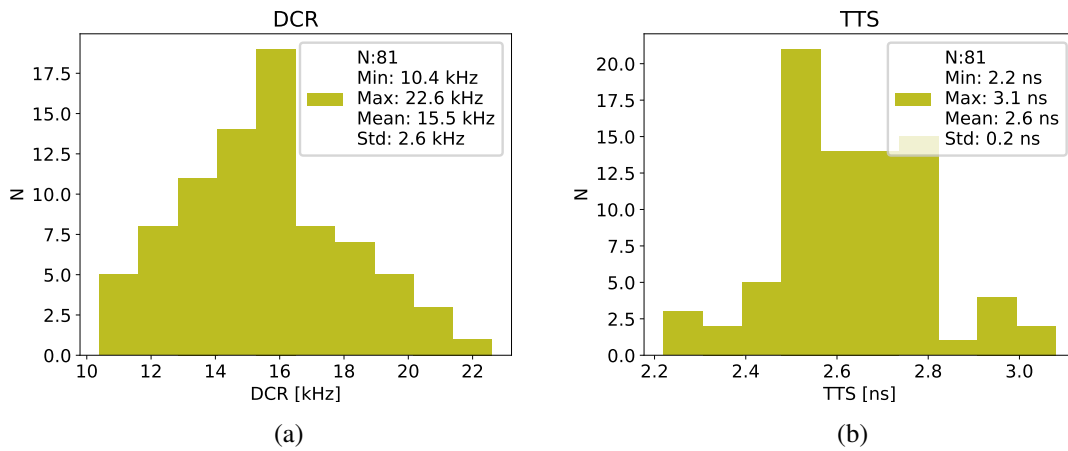


Figure 4: Distribution of PMT parameters as measured by Hamamatsu Photonics: (a) dark count rate, (b) transit time spread (full width at half maximum (FWHM)).

to the voltage. This gives the maximum ground trace thickness. Except for one 10 nF/6 kV capacitor all components are Surface Mount Technology (SMT) types. The base itself gets soldered to the connector of the PMT.

4.3 High Voltage Board

The high voltage board hosts a high voltage module [7]. The decoupling of the signal from the HV is done on this board as well. In order to protect the subsequent components, two gas discharge tubes are added to this board. They limit the voltage to a maximum of 70 V. To prevent charge-up

of the secondary side of the decoupling capacitor, a high ohmic discharge resistor is installed. The influence on the signal by the discharge resistor and tubes is negligible.

4.4 Readout Board

The ROB is the main board in the readout chain (cf. Figure 5). It digitizes the signal, provides the timestamps of the waveform packets, and contains the digital processing unit, a Xilinx® Zynq®¹. For dataprocessing, 1 GB of Random-Access Memory (RAM) is connected [8].

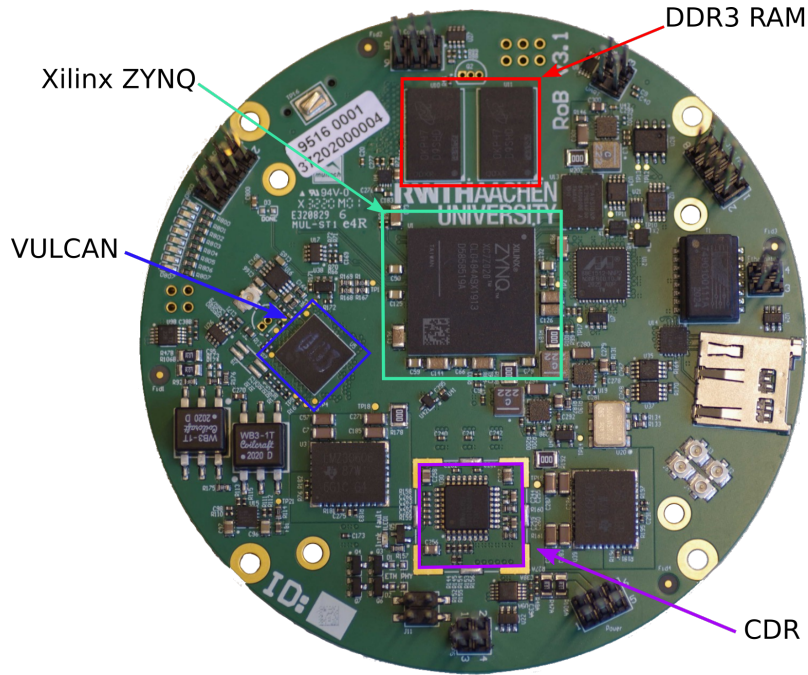


Figure 5: Image of the ROB with important integrated circuits (ICs) highlighted.

All iPMTs are synchronised by a dedicated synchronous link running at 125 Mbit s^{-1} . This link embeds a data stream and a clock via Manchester Coding [9, 142]. On the ROB, this stream is processed by a clock data recovery (CDR) IC (Microchip SY87700AL) and split into a data and clock signal again.

VULCAN

VULCAN [10, 11] is a dedicated PMT frontend and digitization chip developed by the ZEA-2 of the Forschungszentrum Jülich. It can be configured via the Joint Test Action Group (JTAG) interface. *VULCAN* hosts a dedicated phase-locked loop (PLL), which reduces the phase noise of the internal clocks [11]. Inside *OSIRIS* *VULCAN* is used with a sampling rate of 500 MSps.

VULCAN features three identical receivers. They are configured to cover three ranges: high gain (HG), mid gain (MG) and low gain (LG). Using these three ranges, *VULCAN* provides a dynamic range up to 1000 p.e. while maintaining a high resolution at lower charges. The HG and MG channel are using a transimpedance amplifier (TIA) – with the HG channel is configured with a larger amplification. The LG channel measures the voltage across the TIA input.

Each receiver channel serves one 8 bit analog-to-digital converter (ADC). All three channels are digitised in parallel and the data processing logic inside *VULCAN* selects the unsaturated

¹FPGA (Artix-7) and a Dual-Core ARM Cortex-A9 MPCore.

samples with the highest resolution. These samples are forwarded to the Field Programmable Gate Array (FPGA) via a low-voltage differential signaling (LVDS) connection.

4.5 Slow Control and Configuration Unit

The Slow Control and Configuration Unit (SCCU) provides access to all slow monitoring sensors as well as the low level and debugging access to VULCAN and the FPGA.

This board hosts a *STM32F417* microcontroller, which provides through its firmware access to JTAG, Inter-Integrated Circuit (I2C), and Universal Asynchronous Receiver Transmitter (UART) via Ethernet. This board hosts a four port Ethernet switch joining the datastreams from the ROB and the SCCU itself. One port is the uplink to the Surface Board (SB), one connects to the ROB, the third one is for the microcontroller, while the fourth one is not used. The access to JTAG is implemented using the Xilinx Virtual Cable (XVC) [12]. This allows usage of the full FPGA tool chain. Via a custom defined protocol over User Datagram Protocol (UDP), one can access two I2C busses, which are connected to many sensors, which monitor the systems behaviour. The three UART connections are accessible via Teletype Network (Telnet) protocol. For each connection, the baudrate as well as the new line character can be configured remotely. The configuration is stored in the internal EEPROM of the microcontroller. Two of the UARTs are routed to the FPGA and the third one is converted into *RS485* and connected to the HV module.

4.6 Power Over Ethernet

The whole iPMT is powered by Power Over Ethernet (PoE) using PoE Plus (IEEE 802.3at-2009) Class 4. This allows the device to consume up to 25.5 W. Eventhough this limit is never reached by the iPMT, it provides some margin for future extensions of the FPGA functionality.

The PoE signal is rectified using an ideal diode bridge and then fed into the PoE power delivery protocol handling IC. The 48 V rail is connected to two DC/DC converters. One provides an isolated 24 V output for the HV module. The other one is an isolated 5 V regulator supplying the SCCU and the ROB. On these boards, the 5 V is regulated down to the voltages needed on these boards. On the PoE board, a temperature monitoring for the transformer of the 5 V regulator is implemented. The supply voltage and current of the HV module is measured, too. These sensors allow continuous monitoring of the operational conditions.

4.7 Cable

The connection between the iPMT and the Surface Board (SB) is a single CAT5 cable with four twisted wire-pairs. Two pairs are used for the 100 Mbit s^{-1} Ethernet with embedded PoE. The third pair hosts the synchronous connection from the SB to the iPMT, whereas the fourth pair is used for synchronous transmission from the iPMT to the SB.

The whole CAT5 cable is enwrapped in a metal mesh shielding and a high-density polyethylene (HDPE) coat. This outer mantle is compatible with the ultra-pure water in the detector tank. The HDPE coat is filled with a water blocking powder. In case of damage, the powder prevents propagation of water along the cable.

For OSIRIS, a maximum cable length of 25 m is required [4]. During installation of the iPMTs, this cable can be cut to the right length. The technical limit is given by the Ethernet requirements. Typically this limit is 90 m. During the production tests, the cable has been elongated by additional 20 m. No communication problem could be observed with this configuration.

4.8 Potting & Holder

The iPMTs will be submerged in a pool of ultra-pure water. The electronics need to be encapsulated to protect it from contact with water and to keep the water clean. The maximum water depth in OSIRIS is 9 m, which is equal to a maximum water pressure of 0.9 bar the iPMT has to withstand. Since this pressure is low and the PMTs are separated sufficiently, implosion protection is not necessary.

The electronics-stack is encapsulated inside a stainless steel shell. To ensure proper cooling of all electronics boards, this shell is filled with white oil. Via convection, the oil transports the heat from the electronics to the shell, where it gets transferred to the surrounding water. The water in the OSIRIS tank is kept at a stable temperature of about 21 °C.

A Poly(methyl methacrylate) (PMMA) ring is glued to the neck of the PMT. The electronics is mounted on the back of the PMT, the shell is glued to the PMMA ring and filled with oil (cf. to [13] for details of the potting). The oil expands under heating. If no countermeasures are taken, this expansion will damage the electronics. An air-filled HDPE bottle is placed inside the shell to absorb the expansion of the oil.

Special measures have been taken to seal the joint between the cable and the shell. In the region, where the cable enters the shell, all wires are stripped down to the bare copper. For isolation, the cable is embedded in a low viscosity epoxy. It stops creeping of oil or water along the wires in both directions.

The location of the items described above can be seen in Figure 6. The whole iPMT is mounted together with its electromagnetic shield [14] in a stainless steel holder. This holder fixes the position and orientation of the iPMT within OSIRIS. For further support of the PMT, four clamps, made from HDPE, are located around the equator.

5 Surface Board

The main purpose of the Surface Board (SB) is the synchronisation of all iPMTs. Each SB hosts eight cards (Connector Boards) which can connect to six iPMTs each (cf. Figure 7). In total, up to 48 iPMTs can be connected to a single SB. For OSIRIS, two SBs are needed. One SB acts as a *master* and provides the *slave* SB with a clock and a datastream, which is forwarded without any further processing.

After the cables from the iPMTs arrive at the SB, their Ethernet pairs are passively separated from the synchronous ones and further forwarded to a commercial Ethernet switch. The synchronous connection to the iPMT can be divided into a downlink (SB to iPMT) and an uplink with the reverse direction. All downlinks are fed with the same signal, which is generated by a single output of a Xilinx® Zynq® on the SB. This signal is distributed by clock splitters to the cable drivers of all iPMTs. For the uplinks, the signal of the iPMT is routed from the cable receiver to a dedicated input for each iPMT. This creates the possibility to measure the length of the cable by injecting a pulse on the downlink and measuring the travel time, when looped back inside the iPMT. The link integrity can be measured using pseudorandom bitstream (PRBS).

Programming the Zynq® and monitoring temperatures, voltages etc. on the SB, is done by one SCCU using JTAG and I2C. In addition, the UARTs of the SCCU are connected to the Zynq® for monitoring and debug purposes.

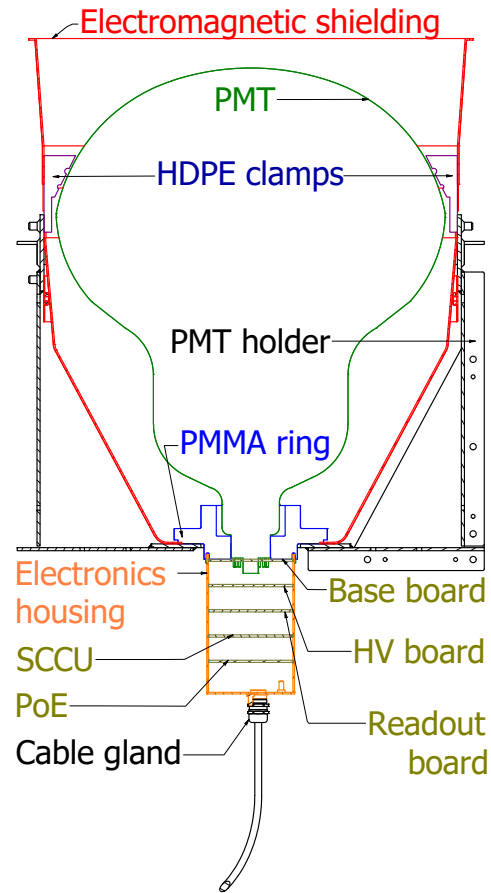


Figure 6: Overview of the iPMT assembly.

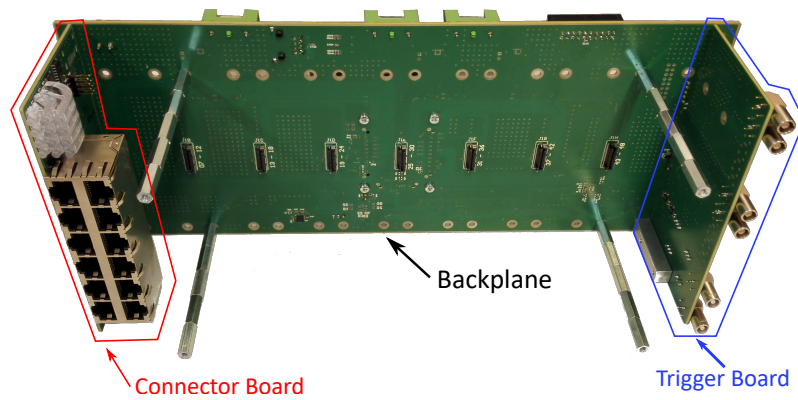


Figure 7: Image of the SB with one Connector board and one Trigger Board.

5.1 LED & Laser Trigger

Each SB provides two independent periodic trigger outputs via a Trigger Board. The trigger rate can be adjusted in a range from 120 mHz to 2.6 MHz. The width of the output pulse can be configured from 16 ns to 496 ns. The outputs are used to trigger light emission from the Laser and LED calibration systems within OSIRIS. A maximal rate of 10 kHz for the laser trigger is

expected [4]. Each output pulse is tagged with a timestamp. This information is sent via Ethernet to the DAQ, where this information is used to form calibration events.

5.2 Synchronisation

All iPMTs are supplied with the identical synchronous datastream with a bitrate of 125 Mbit s^{-1} . A Manchester code is used on the stream which reduces the data rate to 62.5 Mbit s^{-1} . A 125 MHz clock is recovered from the datastream on the ROB by the CDR. The recovered clock is used as reference clock for VULCAN. By using the same frequency on all iPMTs, a frequency synchronisation is achieved (syntonization). Via the embedded datastream the iPMTs are partially synchronised. After this partial synchronisation, a time offset, which is dominated by the cable length difference between the iPMTs, remains. This offset can be determined by measurements of the electrical cable length or using pulsed Laser illumination events. A combination of both methods will provide a full synchronisation of all iPMTs.

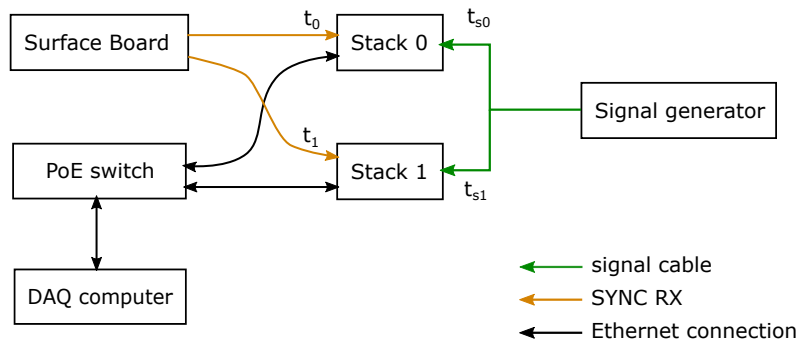


Figure 8: Sketch of the synchronisation setup. The different cable lengths to the electronics stacks (Stack 0 and Stack 1) are represented by the signal travel times t_0 and t_1 .

For testing the partial synchronisation, two half stacks (PoE-Board, SCCU and ROB) are connected to a pulse generator as a signal source. The cable length to both stacks is not matched (cf. Figure 8). When the signal generator creates a pulse, this gets recorded by both stacks. Each stack tags this event with its own timestamp. Figure 9a shows part of a single recorded waveform. To determine the proper timestamp, a linear function is fitted to the rising edge. The time when this interpolation crosses 100 LSB is used as the event time t_{s0} and t_{s1} . Figure 9b shows the difference between both event times against the measurement time. The total measurement time shown in Figure 9b is divided into six times 2 h due to file size constraints. The mean synchronisation difference between both used half-stacks is $(20.84 \pm 0.28) \text{ ns}$. The difference of 20.84 ns is determined by the different cable length. More relevant is the variation of the synchronisation over time, characterised by a standard deviation of 0.28 ns. It is well below the PMT's intrinsic TTS of about 1.1 ns².

6 Slowcontrol of the iPMT system

In order to control all different parts of the iPMT, an implementation based on Experimental Physics and Industrial Control System (EPICS) [15] version 3.14.12.7 has been chosen.

²Figure 4b states a mean TTS of 2.6 ns as FWHM. With the assumption of a Gaussian distribution this number converts to a standard deviation of 1.1 ns.

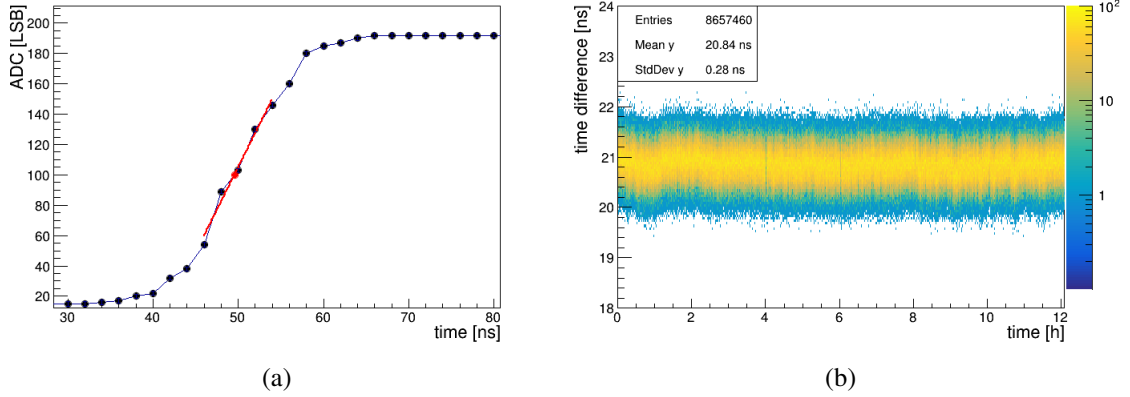


Figure 9: (a) Zoom of a recorded waveform. (b) Histogram of the synchronisation difference against the measurement time.

For each subsystem, like I2C or HV, a dedicated Input / Output Controller (IOC) handles the communication to the iPMT using a custom implementation. Most of the endpoints are handled by the SCCU. The conversion of the raw data into physical values is done by EPICS conversion settings. The whole iPMT can be monitored and controlled via EPICS. It is possible to use a graphical interface as well as scripts to interact with the iPMTs.

The initial values, limits, and alarm settings of each record are derived from a *MySQL* database. Each iPMT can be configured individually. Most of the limits require tuning during the commissioning of OSIRIS. Hence there is a default – fail safe – configuration in the database, which is used in case that no dedicated values are set for an iPMT.

7 Performance of a single iPMT

In this section the representative performance of a single iPMT is shown. For the following measurements, the iPMT has been placed in a magnetic shielding box. An LED illuminates the photo cathode with short pulses of low intensity. LED and iPMT share a common trigger. The response of the iPMT to the light emission is recorded and analysed. For studies of the single photo electron signal, the light intensity of the LED has been tuned such that a pulse is observable in about 10 % of all recorded events. The synchronous detection of two or more photons is highly suppressed.

Only those waveforms are processed whose average baseline in the baseline window (cf. Figure 10) – from 108 ns to 168 ns – is in a range of $\pm 1\sigma$ around the mean average baseline. The accepted average baseline values are 18.55 LSB to 20.70 LSB. By using this cut, the simple charge integration method works reliably and baseline fluctuations from earlier hits are rejected. Using a more advanced waveform reconstruction algorithm would supersede this cut.

7.1 Charge characteristics

To analyse the charge, the waveform is corrected for the baseline, first. The average of the samples in the baseline window is subtracted from all samples. The charge integration window ranges from 184 ns to 244 ns (cf. Figure 10). The histogram of these waveform integrals are shown in

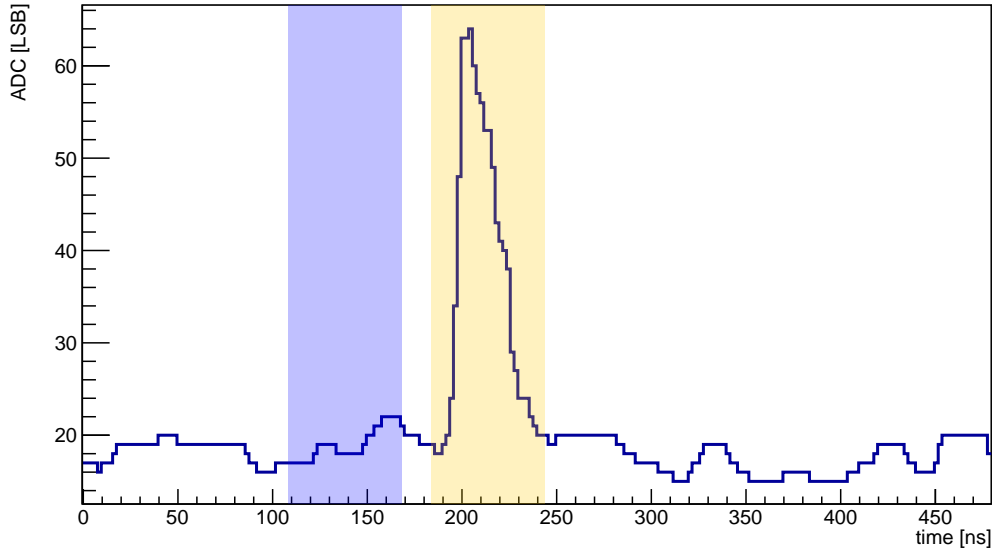


Figure 10: Exemplary waveform of a photo electron equivalent (p.e.) with the baseline window marked in blue and the charge integration window marked in yellow.

Figure 11. It can be seen, that a tiny fraction of events with two p.e. exists in the measurement as well.

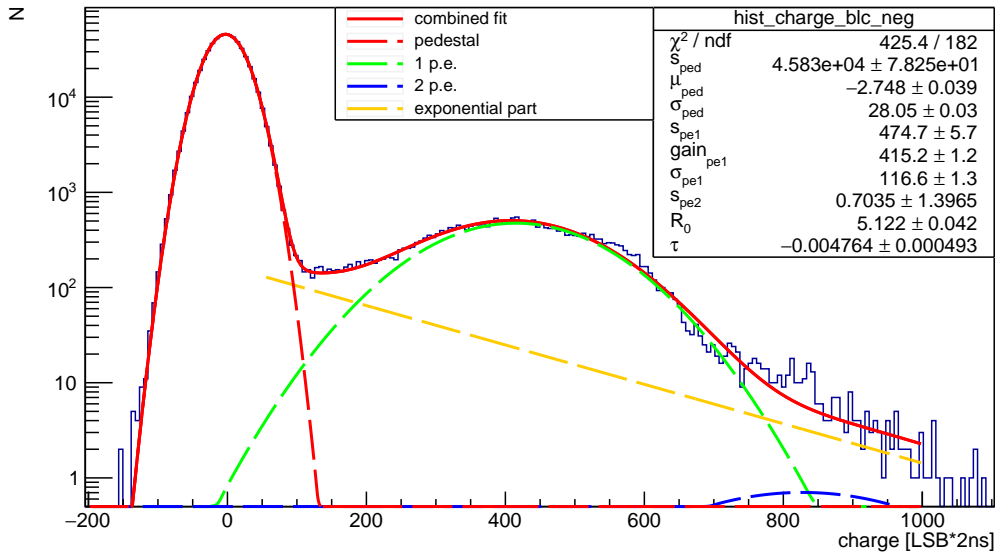


Figure 11: Single photo electron equivalent charge spectrum.

The charge histogram is fitted with Equation 7.1 to extract the gain and other parameters.

$$f_{\text{fit}}(x) = f_{\text{ped}}(x) + f_{\text{pe1}}(x) + f_{\text{pe2}}(x) + f_{\text{exp}}(x) \quad (7.1)$$

$$f_{\text{ped}}(x) = s_{\text{ped}} \cdot e^{-0.5 \cdot ((x - \mu_{\text{ped}}) / \sigma_{\text{ped}})^2} \quad (7.2)$$

$$f_{\text{pe1}}(x) = s_{\text{pe1}} \cdot e^{-0.5 \cdot ((x - (\mu_{\text{ped}} + \text{gain}_{\text{pe1}})) / \sigma_{\text{pe1}})^2} \quad (7.3)$$

$$f_{\text{pe2}}(x) = s_{\text{pe2}} \cdot e^{-0.5 \cdot ((x - (\mu_{\text{ped}} + 2 \cdot \text{gain}_{\text{pe1}})) / (\sqrt{2} \sigma_{\text{pe1}}))^2} \quad (7.4)$$

$$f_{\text{exp}}(x) = \begin{cases} e^{R_0 + \tau \cdot (x - x_v)} & \text{if } x > x_v \\ 0 & \text{otherwise} \end{cases} \quad (7.5)$$

$f_{\text{ped}}(x)$ is a Gaussian component to model the noise, also denoted as pedestal or noise peak. $f_{\text{pe1}}(x)$ and $f_{\text{pe2}}(x)$ are Gaussian functions that describe the charge signals corresponding to one, respective two photo electron equivalents. Since the PMT is a linear amplifier for this low number of p.e., the respective Gaussian mean values are correlated via the variables gain_{pe1} and σ_{pe1} . $f_{\text{exp}}(x)$ is an empirical approach to include other effects into the model to better describe especially the region between pedestal peak and single p.e. peak. The variable x_v is the starting point of this fit on the falling edge of the pedestal peak [8, 16]. The signal to noise ratio (SNR) is given by

$$\text{SNR}_{\text{charge}} = \frac{\text{gain}_{\text{pe1}}}{\sigma_{\text{ped}}} = 14.802 \pm 0.046. \quad (7.6)$$

The noise – in terms of charge – is $\frac{1}{\text{SNR}} = 0.07$ p.e. wide. The charge resolution is calculated as

$$\text{Resolution}_{\text{charge}} = \frac{\sigma_{\text{pe1}}}{\text{gain}_{\text{pe1}}} = (28.08 \pm 0.32) \%. \quad (7.7)$$

The charge resolution is not fully determined by the readout electronics. The amplification process inside the PMT limits this value [17].

From the fit (Equation 7.1), the peak to valley ratio can be determined. It is calculated from the height of the single p.e. peak divided by the number of entries in the valley between the single p.e. peak and the noise peak. For this measurement the value is 3.55, compared to the value of 3.08 measured by the vendor.

7.2 Characteristics of the waveform maximum

This study is done using the raw ADC waveforms without any additional calibration. A distribution of the maximum ADC value within the integration window is shown in Figure 12. Those waveforms which have a charge of $\pm 1\sigma$ around the single p.e. peak (see Figure 11) are plotted in red. From this distribution it can be seen that the single p.e. maximum is on average (51.8 ± 6.0) LSB. With the baseline of (19.6 ± 2.4) LSB, the baseline corrected maximum of a single p.e. is (32.21 ± 5.50) LSB. Using these values, the dynamic range of the high gain receiver with a full scale value $\text{FS}_{\text{HG}} = 255$ LSB can be calculated as

$$N_{\text{PE, HG}} = \frac{\text{FS}_{\text{HG}} - \text{baseline}_{\text{HG}}}{\text{maximum}_{\text{SPE, HG}} - \text{baseline}_{\text{HG}}} = (7.31 \pm 1.44) \text{ p.e.} \quad (7.8)$$

As for the charge, the SNR can be calculated accordingly to

$$\text{SNR}_{\text{maximum}} = \frac{\text{maximum}_{\text{SPE, HG}} - \text{baseline}_{\text{HG}}}{\sigma_{\text{baseline}}} = 13.38. \quad (7.9)$$

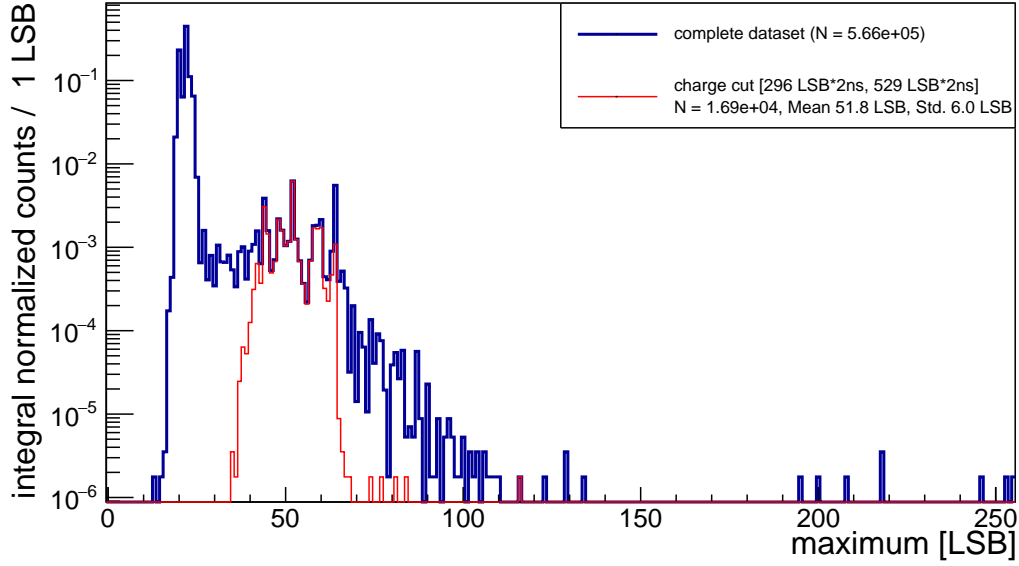


Figure 12: Maximum distribution in charge integration window.

This value is comparable to the charge based value. The resolution can also be derived from the measurement shown in Figure 12 as

$$\text{Resolution}_{\text{maximum}} = \frac{\sigma_{\text{ampl}}}{\text{maximum}_{\text{SPE, HG}} - \text{baseline}_{\text{HG}}} = 18.63\% . \quad (7.10)$$

The resolution of the waveform maximum is less than the charge resolution. But for the maximum only the highest value inside the integration window is used. For the charge, all information from the whole pulse is used. Using a more dedicated waveform reconstruction algorithm might increase the maximum resolution as well.

7.3 Self triggered charge spectrum

In OSIRIS, the iPMTs operate in self-triggered mode. They send out a waveform with a timestamp once their local trigger condition is met. With this acquisition mode, a charge spectrum can be recorded as well. Figure 14 depicts multiple charge spectra recorded with increasing trigger thresholds. It starts at the lowest trigger threshold, which can be recorded without data loss. The charge spectrum obtained with the external trigger is plotted for comparison, too. The trigger thresholds are given in raw ADC counts. After subtraction of the baseline (19.59 LSB), the minimal pulse height can be derived, which is accepted with this setting. Figure 14 shows that the noise suppression increases with the trigger threshold. However, there are still few noise events remaining, which cause a peak between 0 LSB · 2ns to 100 LSB · 2ns. These events have a damped oscillation signature of unknown source as shown in Figure 13. With increasing trigger threshold, the detection threshold in terms of light intensity increases as well.

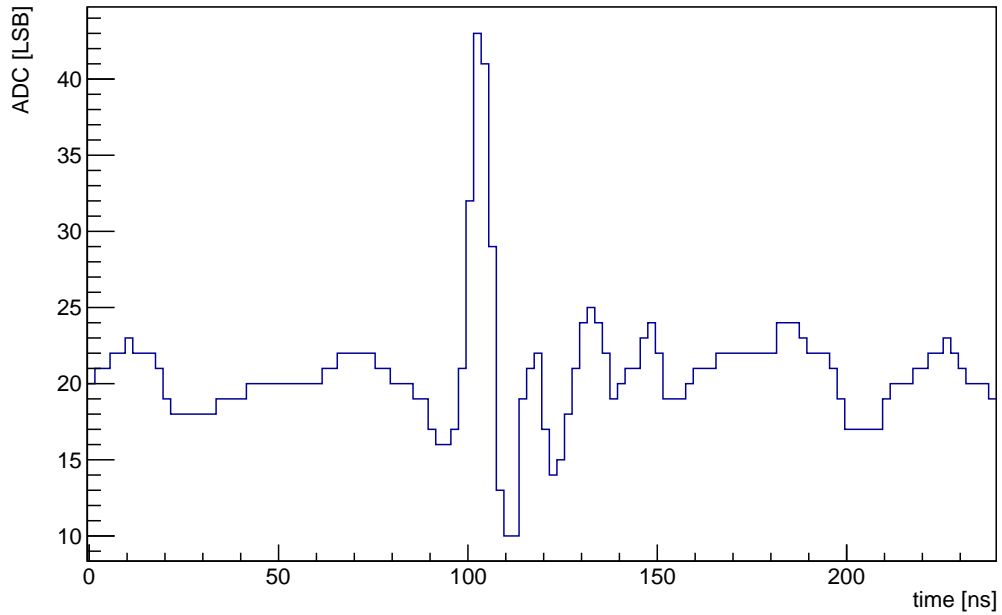


Figure 13: Example of a waveform which contributes to the noise in the self-triggered charge spectrum.

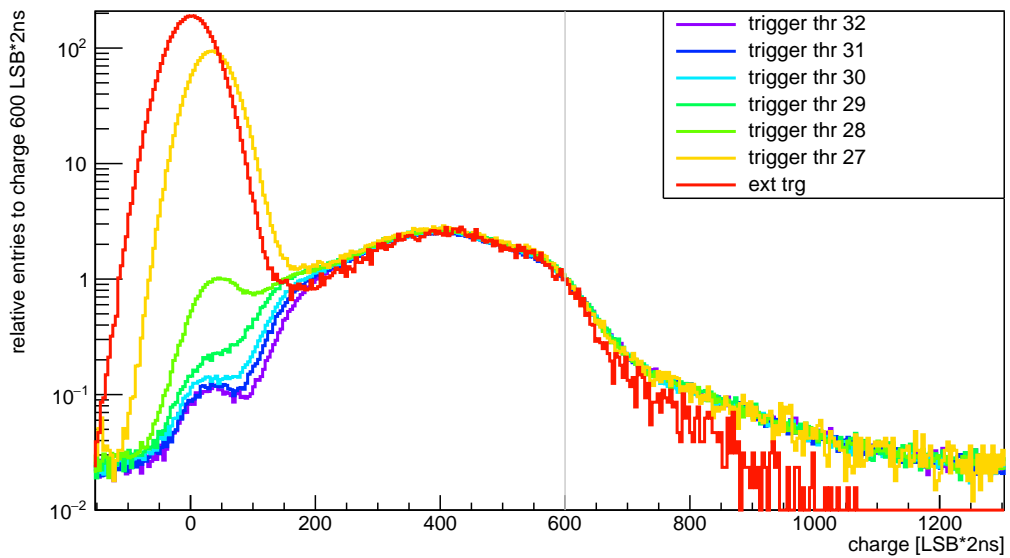


Figure 14: Charge spectra externally triggered and self-triggered. All different spectra are normalised to $600 \text{ LSB} \cdot 2\text{ns}$.

8 Summary / Conclusions

The iPMT concept is a novel PMT readout concept based on the close integration of the PMT and electronics. We presented a detailed description of the system components. It is shown that a partial synchronisation can be achieved, which has a sufficiently low uncertainty. The performance of one exemplary iPMT is presented, focusing on low light level characteristics. In the charge performance this iPMT achieved a signal to noise ratio of 14.802 ± 0.046 and a resolution of $(28.08 \pm 0.32) \%$ for single photon events.

For OSIRIS, 75 iPMTs have been successfully produced, tested and shipped to the JUNO site for installation.

Acknowledgments

This work was supported by the Deutsche Forschungsgemeinschaft (DFG), the Helmholtz Association, and the Cluster of Excellence PRISMA+ in Germany.

References

- [1] F. An, G. An, Q. An, V. Antonelli, E. Baussan, J. Beacom et al., *Neutrino physics with JUNO*, *Journal of Physics G: Nuclear and Particle Physics* **43** (2016) 030401.
- [2] A. Abusleme, T. Adam, S. Ahmad, R. Ahmed, S. Aiello, M. Akram et al., *Radioactivity control strategy for the JUNO detector*, *Journal of High Energy Physics* **2021** (2021) 102 (2021).
- [3] L. Bieger, T. Birkenfeld, D. Blum, W. Depnering, T. Enqvist, H. Enzmann et al., *Potential for a precision measurement of solar pp neutrinos in the Serappis experiment*, *The European Physical Journal C* **82** (2022) .
- [4] A. Abusleme, T. Adam, S. Ahmad, R. Ahmed, S. Aiello, M. Akram et al., *The design and sensitivity of JUNO's scintillator radiopurity pre-detector OSIRIS*, *The European Physical Journal C* **81** (2021) 973.
- [5] G. Alimonti, C. Arpesella, H. Back, M. Balata, D. Bartolomei, A. de Bellefon et al., *The Borexino detector at the Laboratori Nazionali del Gran Sasso*, *Nuclear Instruments and Methods in Physics Research Section A: Accelerators, Spectrometers, Detectors and Associated Equipment* **600** (2009) 568–593.
- [6] S. Yamada, K. Awai, Y. Hayato, K. Kaneyuki, Y. Kouzuma, S. Nakayama et al., *Commissioning of the New Electronics and Online System for the Super-Kamiokande Experiment*, *IEEE Transactions on Nuclear Science* **57** (2010) 428.
- [7] M. Bellato, A. Bergnoli, A. Brugnera, S. Chen, Z. Chen, B. Clerbaux et al., *Embedded readout electronics R&D for the large PMTs in the JUNO experiment*, *Nuclear Instruments and Methods in Physics Research Section A: Accelerators, Spectrometers, Detectors and Associated Equipment* **985** (2021) 164600.
- [8] C. Wyszotki, *Development and production of an intelligent PMT readout system for OSIRIS*, Dissertation, RWTH Aachen University, 2023. 10.18154/RWTH-2023-00743.
- [9] W. Stallings, *Data and computer communications*, Pearson/Prentice Hall, eight ed. (2007).
- [10] P. Muralidharan, *Digital Signal Processing and Mixed Signal Control of Receiver Circuitry for Large-Scale Particle Detectors*, Dissertation, Universität Duisburg, Jülich, 2020.
- [11] N. Parkalian, *Configurable frequency synthesizer for large scale physics experiments*, Dissertation, Universität Duisburg, Jülich, 2019.

- [12] “XilinxVirtualCable.” <https://github.com/Xilinx/XilinxVirtualCable>.
- [13] F. Gao, *Design, production and test of intelligent PMTs for the JUNO experiment*, Dissertation, RWTH Aachen University, 2022. 10.18154/RWTH-2022-08620.
- [14] O. Smirnov, D. Korablev, A. Sotnikov, A. Stahl, J. Steinmann, V. Khudyakov et al., *Magnetic shielding for large photoelectron multipliers for the osiris facility of the junos detector*, *Journal of Instrumentation* **18** (2023) P04015.
- [15] “Experimental Physics and Industrial Control System.” <http://www.aps.anl.gov/epics/>.
- [16] C. Bauer, E. Borger, R. Hofacker, K. Jänner, F. Kaether, C. Langbrandtner et al., *Qualification tests of 474 photomultiplier tubes for the inner detector of the Double Chooz experiment*, *Journal of Instrumentation* **6** (2011) P06008.
- [17] T. Kuhlbusch, *Vermessung und Simulation von Photomultiplier Tubes für das JUNO-Projekt*, Bachelor’s Thesis, RWTH Aachen University, September, 2017.